LAWRENCE
LIVERMORE
NATIONAL
LABORATORY

LLNL-JRNL-453431

An experimental and kinetic modeling study of n-octane and 2-methylheptane in an opposed-flow diffusion flame

S. M. Sarathy , C. Yeung, C. K. Westbrook, W. J. Pitz, M. Mehl, M. J. Thomson

September 7, 2010

Combustion and Flame

Disclaimer

An experimental and kinetic modeling study of *n*-octane and 2-methylheptane in an opposed-flow diffusion flame

S. M. Sarathy[1*], C. Yeung[2], C.K. Westbrook[1], W.J. Pitz[1], M. Mehl[1], M.J. Thomson[2]

[1] Physical and Life Sciences Directorate, Lawrence Livermore National Laboratory

[2] Department of Mechanical & Industrial Engineering, University of Toronto

Submitted to Combustion and Flame as a full length article

* Corresponding Author:

S. Mani Sarathy

Physical and Life Sciences Directorate

Lawrence Livermore National Laboratory

7000 East Avenue, L-367

Livermore, CA 94551

USA

Email: sarathy1@llnl.gov

Phone: 925-423-6011

ABSTRACT

Fischer-Tropsch (FT) fuels derived from biomass syngas are renewable fuels that can replace conventional petroleum fuels in jet engine and diesel engine applications. FT fuels typically contain a high concentration of lightly methylated *iso*-alkanes, whereas petroleum derived jet and diesel fuels contain large fractions of *n*-alkanes, cycloalkanes, and aromatics plus some lightly methylated *iso*-alkanes. In order to better understand the combustion characteristics of FT and petroleum fuels, this study presents new experimental data for 2-methylheptane and *n*-octane in an opposed-flow diffusion flame. The high temperature oxidation of 2-methylheptane and *n*-octane has been modeled using an extended transport database and a reaction mechanism consisting of 3081 reactions involving 608 species. The proposed model shows good qualitative and quantitative agreement with the experimental data. The measured and predicted concentrations of 1-alkenes and ethylene are higher in the *n*-octane flame, while the concentrations of *iso*-alkenes (especially *iso*-butene) and propene are higher in the 2-methylheptane flame. The proposed chemical kinetic model is used to delineate the reactions pathways leading to these observed differences in product species concentrations. An uncertainty analysis was conducted to assess experimental and modeling uncertainties. The results indicate that the simulations are sensitive to the transport parameters used to calculate fuel diffusivity.

INTRODUCTION

The increasing demand for gasoline, diesel, and jet fuels has put significant pressure on the supply of conventional petroleum feedstock. Therefore, the production of transportation fuels from alternative feedstock is necessary for energy security. Fischer-Tropsch (FT) liquid fuels are one class of fuels that can be produced from other hydrocarbon sources, such as coal and natural gas. The commercialization of FT fuels began in the 1930s, but only in the last 15 years has there been a significant investment into new production facilities [1]. Since FT fuels can be generated from any syngas ($CO + H_2$) source [2], the use of gasified biomass to produce FT fuels provides the opportunity for a renewable fuel with significant environmental benefits.

The production of FT fuels initially creates long chain *n*-alkanes (i.e., paraffinic waxes), some of which are partially isomerized to meet jet fuel density and freeze point specifications [2]. Detailed chemical analysis of a natural gas derived FT fuel known as S-8 indicates a mixture of C_7 to C_{18} linear alkanes and *iso*-alkanes with one or two methyl branches [3,4]. Gokulakrishnan et al. [6] have reported the high temperature ignition characteristics of S-8. Huber et al. [5] have proposed an S-8 surrogate that well produces the thermophysical properties of the real fuel; two of the principal components in the surrogate are 3-methyldecane and 2,6-dimethyloctane. Additionally, Colket et al. [7] proposed 2-methylundecane as a surrogate for the *iso*-alkanes in jet fuel.

The goal of the present study is to better understand the combustion properties of lightly branched alkanes. The focus is on 2-methylheptane (C_8H_{18}-2, refer to Figure 1), since this is the simplest *iso*-alkane present in S-8 [3,4]. This paper presents a chemical kinetic model for the high temperature combustion of 2-methylheptane and validates it against opposed-flow diffusion flame experiments. Experimental and modeling data for *n*-octane is also included to understand the key differences in the combustion of straight alkanes and 2-methylalkanes. The current work is the first step towards a detailed high temperature and low temperature chemical kinetic model for C_7 to C_{20} 2-methylalkanes.

Combustion research on 2-methylalkanes

There has been limited research on the fundamental combustion properties of 2-methylalkanes. The smallest 2-methylalkane, *iso*-butane (2-methylpropane, iC_4H_{10}), was studied by Wilk et al. [8] in an internal combustion engine, and the results were modeled using a detailed chemical kinetic mechanism. At a given pre-ignition temperature, *iso*-butane is shown to be less reactive than *n*-butane because *iso*-butyl radicals cannot undergo rapid RO_2 isomerization

reactions that lead to chain branching. Ogura et al. [9] studied *iso*-butane in a shock tube at high temperatures of 1200-1600K, 1.7-2.4 atm, and an equivalence ratio of 0.72. They concluded that *iso*-butane has longer ignition delay times than *n*-butane because of the greater amount of propene production, which leads to the resonantly stabilized allyl (C_3H_5) radical. Oehlschlaeger et al. [10] provided shock tube measurements and OH concentration time histories for *iso*-butane and *iso*-pentane (2-methylbutane, iC_5H_{12}) spanning 1117-2009 K, 1.10-12.58 atm, and equivalence ratios of 0.25-2. They explain that *iso*-alkanes are less reactive than *n*-alkanes because the greater number of primary C-H bonds leads to more methyl production, which scavenge reactive OH radicals. Recently, Healy et al. [11] presented ignition delay times and an improved chemical kinetic model for *iso*-butane spanning 590 to 1567 K, 1-30 atm, and equivalence ratios of 0.3-2. For other *iso*-alkanes, Burcat et al. [12] found that the high temperature ignitions kinetics of 2-methylpentane (C_6H_{14}-2) were similar to *n*-hexane at1175-1772 K and 2-4.6 atm. Their chemical kinetic model indicates that unimolecular decomposition of 2-methylpentane into *n*-propyl (nC_3H_7) and *iso*-propyl (iC_3H_7) is the key initiation step during ignition at high temperature (e.g., 1500K).

Several experimental and kinetic modeling studies have been performed on 2-methylhexane (C_7H_{16}-2). Westbrook et al. [13] proposed a high temperature model for all nine isomers of heptane, including 2-methylhexane. No experimental results were available for model validation; however, high temperature shock tube simulations indicate that 2-methylhexane has similar ignition delay times to *n*-heptane. H-atom abstraction from the fuel is the primary initiating step, except at the highest temperatures where unimolecular decomposition becomes important. A subsequent study by Westbrook et al. [14] presented a detailed chemical mechanism including low temperature chemistry for 2-methylhexane and used rapid compression machine data from Griffiths et al. [15] for validation. Their simulations indicate that 2-methylhexane is noticeably slower to react than *n*-heptane in the low and intermediate temperature regimes (e.g., 650-900 K). Silke et al. [16] also reported that 2-methylhexane is less reactive than *n*-heptane in rapid compression experiments from 650-950 K at 15 atm.

Currently, the largest 2-methylalkane to be studied is 2-methylheptane (C_8H_{18}-2). Kahandwala et al. [17] reported high temperature shock tube ignition delays and particulate matter (PM) emissions for jet fuel (JP-8), F-T jet fuel (S-8), *n*-heptane/toluene mixture (surrogate JP-8), and 2-methylheptane (surrogate S-8). They found that both S-8 and 2-methylheptane produce less PM emissions than the real and surrogate JP-8. However, no differences in ignition

delay times were observed for both actual and surrogate JP-8 and S-8 at the high temperatures studied (i.e., 1100-1600 K).

Experimental Methods

Opposed-flow Diffusion Flame

The experimental setup is similar to that described earlier by Sarathy et al. [18]. The setup consists of two identical flat flame burners with circular burner ports of diameter 25.4 mm, facing each other and spaced 20 mm apart. A fuel mixture of 98.14% N_2 and 1.86% fuel (99% pure *n*-octane or 98% pure *2*-methylheptane) is fed through the bottom port at a mass flux rate of 0.015 g/cm^2-sec, while an oxidizer mixture of 42.25% O_2 and 57.75% N_2 is fed through the top port at a mass flux rate of 0.014 g/cm^2-sec. At these plug flow conditions, the Reynold's Number at the fuel port exit is in the laminar flow regime (i.e., Re = 176), the flame is on the fuel side of the stagnation plane, and the fuel side strain rate is approximately 36 s^{-1}. To prepare the fuel mixture, a peristaltic pump delivered the fuel to an ultrasonic atomizer which sprays the liquid fuel into a stream of N_2 gas. The gaseous fuel mixture is delivered to the burner via heated stainless steel tubing. The temperatures of the gases exiting the top and bottom burner ports were 420 K and 350 K, respectively. The mass flow controllers used to meter the delivery of nitrogen, oxygen, and air have a manufacturer reported error of ±1%. The pump used to deliver the liquid fuel was calibrated before each experiment to an accuracy of ±2%.

The gas sampling system in these experiments consists of a fused-silica microprobe (0.20 mm internal diameter, 0.32 mm outer diameter, and 5 cm length) connected to a dual-stage pump with heated heads (420 K) and PTFE diaphragms to prevent the condensation of high boiling point compounds. The suction side of the sampling system consists of heated stainless steel tubing (6.35 mm internal diameter and 2 m length) and a pressure gauge connected to the quartz microprobe. An absolute pressure of 4-6 kPa was measured downstream of the microprobe. This is sufficient to quench most reactions and ensure accurate data on flame composition. The compression side of the pump delivers the samples to the analytical instruments via heated stainless steel tubing (6.35 mm internal diameter and 2 m length). The temperature of all heated surfaces is 420 K.

Analytical techniques used to analyze the species in the sample includes: GC/FID with an HP-Al/S PLOT column for C_1 to C_8 hydrocarbons and GC/TCD for CO and CO_2. Temperature measurements were obtained using both a 100 μm and a 250 μm wire diameter R-type thermocouple (uncoated Pt/Pt-13%Rh) in an apparatus similar to that used by McEnally et al.

[19]. This apparatus was unable to accurately measure temperatures on the oxidizer-rich side of the flame, so measurements above 11 mm from the fuel port are not reported. The measured temperatures were corrected for radiation losses using the method described by Shaddix [20]. The Nusselt number was calculated assuming a spherical bead of the same diameter as the wires and Prandtl numbers for pure N_2 at 398 K. The emissivity was obtained from [21] and the thermal conductivity of air was from [22]. The possibility of catalytic reactions occurring on the uncoated thermocouple wires is acknowledged [20], but were not corrected. Fluctuations of ± 50-80 K were observed in the hot regions near the flame front (i..e., above 1300 K), so we report the 10 second average. We estimate a maximum error of ±10% in the temperature measurements, and the precision of species measurements is estimated to be ±15%.

Computational Methods

The kinetic modeling for 2-methylheptane and *n*-octane was performed using the CHEMKIN PRO modeling package [23]. The opposed-flow diffusion flame was modeled using the OPPDIF code. The simulations used mixture-averaged transport and included thermal diffusion. The solution was assumed grid-independent when increasing the number of grid points did not change the simulated temperature and species profiles (i.e., 200 grid points). Solutions with approximately 270 grid points are reported in this paper.

The data files for the simulation include a detailed chemical kinetic reaction mechanism, a dataset of thermochemical properties, and a dataset of transport properties. The entire model consists of 3081 reactions involving 608 species. These input files are available as supplemental material to this publication and from our website at:
https://www-pls.llnl.gov/?url=science_and_technology-chemistry-combustion.

Chemical Kinetic Mechanism

The chemical kinetic reaction mechanism for 2-methylheptane builds upon previous *n*-alkane [24] and *iso*-octane mechanisms [25,26]. The base mechanism consists of comprehensive low temperature and high temperature reactions for C_0 to C_7 species from [25,26] species plus high temperature reactions for *n*-octane from [24]. The present mechanism was then built in a modular fashion, starting with the high temperature reactions for 2-methylhexane described by Westbrook et al. [13]. The high temperature reactions for 2-methylheptane were then written for each of the nine classes described by Curran et al. [27].

1. Unimolecular decomposition
2. H-atom abstraction from the fuel
3. Alkyl radical decomposition
4. Alkyl radical + O_2 to produce alkene and HO_2 directly
5. Alkyl radical isomerization
6. Abstraction reactions from alkenes by OH, H, O, and CH_3
7. Addition of radical species to alkenes
8. Alkenyl radical decomposition
9. Alkene decomposition

2-Methylheptane is denoted as C_8H_{18}-2 in the mechanism (see Figure 1). The carbon chain is labeled numerically (i.e., 1, 2, 3, etc.) such that the location number of the methyl branch is minimized. For 2-methylheptane species, the location of a double bond is identified by a hyphen followed by the number of the first carbon in the double bond (e.g., 2-methyl-3-heptene is C_7H_{14}-3-2). Additional notations are provided to denote radical sites in the molecule. The carbon sites are labeled alphabetically (i.e., a, b, c, etc.) such that the location of the first methyl branch is minimized (see Figure 1). In this way, the 2-methyl-3-heptyl radical is denoted as C_7H_{15}-2c, while the 2-methyl-1-heptyl radical is written as C_7H_{15}-2a.

The reaction rate rules used for each class of reactions are the same as those in the *iso*-octane mechanisms [25,26,28]. For example, H-atom abstraction by OH from the tertiary carbon in 2-methylheptane has the same rate as the analogous reaction in *iso*-octane. Unimolecular decomposition reactions are specified in the reverse direction (i.e., recombination), and the rate of recombining two radicals is assigned. The decomposition rate is computed using the principle of microscopic reversibility. Retroene reactions for 2-methylalkenes were added to the conventional class 9 reactions using the rate expressions from [24].

Thermochemical Data

The THERM [29] software was used to compute the thermodynamic properties of species not present in the *n*-alkane model [24]. The THERM group values are from Benson [30].

Transport Properties

In certain combustion applications, such as the shock tubes, the overall rate is assumed to be kinetically controlled since fuel and air are premixed and combustion is assumed to occur

homogeneously. Therefore, many published models exclude transport property databases. However, the transport processes are rate controlling in laminar diffusion flames. This study obtained the molecular transport parameters for species using a variety of methods. The transport properties for the majority of compounds were already available in a previously published primary reference fuel (PRF) model [25, 26]. The Lennard-Jones (LJ) collision diameter and potential well depth were changed for a number of small species based on the recommendations of Mourits and Rummens [31]. The transport data files contains comments to indicate which species were modified. The transport properties of larger alkane, alkene, alkyl, and alkenyl species were determined as follows. For stable species (e.g., *n*-octane and 2-methylheptane), this study used the correlations developed by Tee, Gotoh, and Stewart [32], as described in Holley and coworkers for hydrocarbons [33], to calculate the LJ collision diameter and potential well depth using the critical pressure (P_c), critical temperature (T_c), and boiling point (T_b) of the species. P_c, T_c, and T_b for stable species were obtained from [33]. The polarizability in cubic Angstroms of stable species was obtained experimentally measured values available in [22]. The dipole moment was obtained from [35]. The index factor which describes the geometry of the molecule was determined from the molecular structure (i.e., 0 for atoms, 1 for linear molecules, and 2 for nonlinear molecules). We assumed that the transport properties are similar for alkanes and alkenes of the same chain length. For alkyl and alkenyl radical species, the transport properties of their stable counterpart were used.

Results and Discussion

The proposed chemical kinetic model was validated against experimental data for *n*-octane and 2-methylheptane in an opposed-flow diffusion flame. The opposed-flow diffusion flame allows us to study the oxidation of these hydrocarbon fuels in a non-premixed flame environment. Temperature and species concentration profiles were obtained by sampling and measuring the product gas at various points between the two burner ports. The measured species included *n*-octane (nC_8H_{18}), 2-methylheptane (C_8H_{18}-2), carbon monoxide (CO), carbon dioxide (CO_2), methane (CH_4), ethane (C_2H_6), ethylene (C_2H_4), acetylene (C_2H_2), propene (C_3H_6), *iso*-butene (iC_4H_8), 1-pentene (C_5H_{10}-1), 3-methyl-1-butene (denoted as 2-methyl-3-butene, C_5H_{10}-3-2), 1-hexene (C_6H_{12}-1), and 4-methyl-1-pentene (denoted in the mechanism as 2-methyl-4-pentene, C_6H_{12}-4-2). The gas chromatography method could not separate 1-butene (1-C_4H_8) from 1,2-propadiene (1,2-C_3H_4), so we report the combined concentration of these two species. The same was done for 1,3-butadiene (1,3-C_4H_6) and propyne (C_3H_4). We did not attempt to

measure oxygenated species such as aldehydes and ketones. Besides the alkenes mentioned above, the analytical system was not designed to measure the isomers of pentene, hexene, heptene, and octene. Species below the experimental limit of quantification (5 PPM) included propane, *n*-butane, 1-butyne, 2-butyne, *trans*-2-butene, *cis*-2-butene, *n*-pentane, and *n*-hexane.

The reported species and temperature profiles were shifted by 0.5 mm away from the fuel port to account for the internal diameter of the microprobe (i.e., 0.2 mm) plus a positioning uncertainty of 0.3 mm, which is a human error introduced when zeroing the sampling probe against the fuel port surface. It is widely accepted to shift species profiles [36] to account for probe-induced or thermocouple-induced perturbations to the flame structure; however, the profiles reported in this study have not been shifted to account for these.

2-Methylheptane Results

Figure 2 displays the measured and predicted species and temperature profiles obtained in the 2-methylheptane opposed-flow diffusion flame. C_6H_{12}-4-2 is not plotted since both peak measured and predicted concentrations are below 100 PPM. The experimental errors in species concentrations are to high for concentrations below 1000 ppm. The experimental results (solid symbols) show that the 2-methylheptane concentration decreases quickly at a distance of 5.5 mm from the fuel port. As the fuel is consumed, the CO and CO_2 concentrations begin rising. All of the fuel is consumed at a distance of approximately 8.25 mm from the fuel port, which corresponds closely to the peak measured temperature (1688 K). The flame front was visually observed at approximately 8.5 mm from the fuel port. Just before the flame front, at around 8 mm from the fuel port, the concentrations of hydrocarbon species reach their peak. Besides CO and CO_2, the most abundant measured species are C_2H_4, C_2H_2, CH_4, and C_3H_6.

The model well reproduces the shape of the experimental temperature and species profiles; however, the experimental data is shifted by about 0.5 mm towards the fuel port. This discrepancy could be resolved by shifting the experimental profiles, which is widely accepted [36]. In the following discussion, the model's quantitative prediction is considered good if the predicted maximum mole fraction is within a factor 1.5 of the measured maximum mole fraction. The model well reproduces the experimentally measured temperature profile, but the maximum measured temperature is more than 100 K higher than the predicted value. A delay (i.e., shift away from the fuel port) in the predicted reactivity of 2-methylheptane is observed. The maximum concentration of CO_2 is well predicted, while the maximum concentration of CO is under predicted by approximately 1.4 times. The model performs well at predicting the peak

measured concentrations of CH_4, C_2H_4, C_2H_2, C_2H_6, 1,3-C_4H_6 + C_3H_4, iC_4H_8, C_5H_{10}-1, and C_5H_{10}-3-2, and 1-C_4H_8 + 1,2-C_3H_4. The peak concentration of C_3H_6 is under predicted by nearly 1.5 times.

n-Octane Results

Figure 3 displays the measured and predicted species and temperature profiles obtained in the *n*-octane opposed-flow diffusion flame. The experimental fuel, CO, CO_2, and temperature profiles are comparable to those of 2-methylheptane. Therefore, both fuels have similar reactivity under the present conditions.

The proposed model well reproduces the shape of the experimental temperature and species profiles, with the same 0.5 mm shift observed as for 2-methylheptane. The model well reproduces the experimentally measured temperature profile, the profile for *n*-octane, and the peak concentration of CO_2. The peak concentration of CO is under predicted by approximately 1.4 times. The model also well predicts the peak measured concentrations of CH_4, C_2H_4, C_2H_2, C_2H_6, 1,3-C_4H_6 + C_3H_4, C_5H_{10}-1, C_6H_{12}-1and 1-C_4H_8 + 1,2-C_3H_4. The maximum concentration of C_3H_6 is under predicted by approximately 1.7 times.

Discussion of 2-methylheptane and n-octane results

Experiments and simulations were conducted to elucidate the differences in combustion between an *n*-alkane and a 2-methyalkane. **Table 1** presents the peak measured and predicted mole fractions in the *n*-octane and 2-methylheptane flames. Considering that the experimental error is ±15%, the two flames have similar concentrations of CO_2, CO, CH_4, C_2H_6, and C_2H_2. Both the experiments and simulations indicate that the 2-methylheptane flame produces more C_3H_6 and 2-methylalkenes (e.g., iC_4H_8, C_5H_{10}-3-2, and C_6H_{12}-4-2) while the *n*-octane flame produces more C_2H_4 and 1-alkenes (e.g., C_5H_{10}-1 and C_6H_{12}-1). The experimental data does not allow us individually quantify 1-C_4H_8, 1,2-C_3H_4, 1,3-C_4H_6, and C_3H_4; however, the model predicts that the *n*-octane flame produces 1-C_4H_8 while the 2-methylheptane flame produces more 1,2-C_3H_4 and 1,3-C_4H_6.

Reaction path analyses were performed using the proposed model to explain the difference observed for the *n*-octane and 2-methylheptane flames. Reaction path analyses were performed at two different temperatures, as follows:

- low temperature, T=805 K, corresponding to approx. 7.2 mm from the fuel port and 21% of the fuel consumed;

- intermediate temperature, T=1185 K, corresponding to 8.1 mm from the fuel port and 80% of the fuel consumed. These conditions also correspond closely to the peak of many hydrocarbon products.

Figure 4 displays the primary reactions paths involved in the consumption of 2-methylheptane at the two aforementioned temperatures, with italic and bold texts referring to low and intermediate temperature conditions, respectively. Percentages corresponding to each pathway are rounded to the nearest whole number. The low temperature analysis provides an understanding of how fuel consumption initiates in the flame. According to the proposed model, H-atom abstraction accounts for the nearly 100% of the fuel consumption, with abstraction being dominated by H atoms, OH radicals, and CH_3 radicals. At intermediate temperatures, the analysis provides an understanding of the reactions occurring near the peak of hydrocarbon products. Again, the fuel consumption is dominated by H-atom abstraction reactions by H atoms, OH radicals, and CH_3 radicals. At high temperatures (e.g., 1500 K, not shown in Figure 4), H-atom abstraction reactions are negligible and the energy is now available to activate unimolecular decomposition reactions. However, the amount of fuel that reaches these conditions is small, so these reactions do not contribute significantly to the formation of product species.

At both low and high temperatures, H-atom abstraction from the tertiary carbon is the most predominant route (20%) because tertiary C-H bonds are weaker than secondary and primary C-H bonds. The abstraction of secondary H atoms is equally distributed amongst the four secondary carbon sites (i.e., 16% each). There are three primary carbon atoms in 2-methylheptane and 5% of the fuel is consumed via H-atom abstraction from each of these sites; however, H-atom abstraction from the two primary carbon atoms near the methyl branch produces the same radical, so this route is effectively doubled (i.e., 10% leads to C_8H_{17}-2a). The fuel radicals formed via H-atom abstraction are primarily consumed via β-scission. Abstraction from the tertiary site eventually leads to the formation of iC_4H_8 and C_2H_4. Fuel radicals with a radical site on a secondary carbon atom can undergo β-scission to form either a 1-alkene or a 2-methylalkene. However, β-scission reactions tend not to favor the formation of a methyl radical, so the routes leading to C_3H_6, C_4H_8-1, and C_5H_{10}-3-2 are predominant. Ethyl (C_2H_5) and *n*-propyl (C_3H_7) appear in a number of pathways, and these eventually lead to the formation of C_2H_4 and C_3H_6.

Figure 5 displays the reactions paths involved in the consumption of *n*-octane. *n*-Octane is a symmetric molecule, so this figure displays pathways for the four possible *n*-octyl radicals. Therefore, the percentages displayed for each pathway are effectively doubled. At both low and intermediate temperatures, H-atom abstraction accounts for the nearly all of the fuel consumption, with abstraction being dominated by H atoms, OH radicals, and CH_3 radicals.

H-atom abstraction from the secondary carbon atoms is the most predominant route because secondary C-H bonds are weaker than primary C-H bonds. The abstraction of secondary H atoms is equally distributed amongst the six secondary carbon sites (i.e., 15% each). H-atom abstraction from the two primary carbon atoms accounts for 9% of the fuel consumption (i.e., 4.5% each). The fuel radicals formed are primarily consumed via β-scission reactions. However, at low temperatures some of the C_8H_{17}-1 radical undergoes isomerization to form C_8H_{17}-4 via 5-membered and 6-membered transition states. The reaction pathways clearly indicate that C_4H_8-1, C_5H_{10}-1, and C_6H_{12}-1 are produced after β-scission of fuel radicals with a radical site on a secondary carbon. C_2H_4 also appears to be formed in nearly every pathway, either directly or via ethyl (C_2H_5) and *n*-propyl (C_3H_7).

As mentioned previously, the 2-methylheptane flame produces more C_3H_6, iC_4H_8, C_5H_{10}-3-2, and C_6H_{12}-4-2, and the *n*-octane flame produces more C_2H_4, 1-C_4H_8, C_5H_{10}-1 and C_6H_{12}-1. The model's reaction pathways clearly display how the combustion of 2-methylheptane leads to significant amounts of propene and *iso*-alkenes, while *n*-octane leads to the formation of ethylene and 1-alkenes. The simulations predict that the 2-methylheptane flame produces more 1,2-C_3H_4 (allene) and 1,3-C_4H_6. These dienes are produced when an H-atom is abstracted from an alkene, and the subsequent alkenyl radical undergoes by β-scission. However, the proposed model simplifies the treatment of H-atom abstraction from alkenes, as described by Curran et al. [27]. A single rate expression is used for H-atom abstraction from primary, secondary, allylic, and vinylic C-H bonds. Furthermore, only one "lumped alkenyl radical" is created when an H-atom is abstracted from various sites on an alkene. Due to these simplifications, we cannot be certain in the model's predicted levels of dienes (i.e., 1,2-C_3H_4 and 1,3-C_4H_6). Additional experiments on diene formation, as well as more detailed modeling for alkene chemistry, such as that presented by Mehl et al. [39,40], are required to improve the proposed chemical kinetic model.

Uncertainty analysis

This section addresses discrepancies between the experimental data and model predicted values by critically assessing potential sources of error. On the experimental side, errors can be

introduced during the supply of reactants to the burner or during sampling. From a modeling perspective, errors can be introduced by incorrect reaction pathways and rate constants, thermochemical data, or transport parameters.

Experimental uncertainties

The slight under prediction of peak species concentrations (e.g., CO, C_2H_4, C_3H_6, etc.) and temperature suggests that the carbon balance in the experimental flame is different from that of the simulated flame. The gaseous reactants (air, oxygen, and nitrogen) were introduced to the burner using mass flow controllers with a manufacturer reported error of 1%, so their flows are considered accurate. The fuel was introduced using a peristaltic pump with an estimated error of 2% (e.g., ± 0.01 mL/min). Extra precautions were taken to confirm that the delivery of reactants to the burner was accurate. All the supply lines were initially tested for leaks. In addition, the fuel supply system was designed and tested to ensure complete vaporization of the fuel, homogeneous mixing with nitrogen, and no fuel condensation in the supply lines. Given these precautions, we are confident in the boundary conditions used for simulating the experiments. Nevertheless, a flame simulation was conducted assuming a 2% (vol.) increase in the liquid flow rate, which correspond to an increase in the fuel stream mole fraction to 1.88% fuel and 98.12% N_2. The additional carbon to the flame slightly increases the maximum predicted temperature (+ 30 K) and species concentrations, but the change is small compared to the magnitude of the initial discrepancies.

Sampling errors may also be a source of discrepancies between the model and experiments. It is noted that the difference between measured and predicted temperatures could be due to catalytic reactions on the thermocouple wires [19], but this was not investigated in the present study. The integrity of the species sampling system was verified by running a numerical reactor simulation with the detailed chemical kinetic model. The sampling system was modeled using three plug flow reactors (PFR) in series, as shown in Figure 6. The combustion products obtained from the flame simulation at 1100 K (i.e., approximately 8 mm from the fuel port) were introduced to the PFR simulation at 30 mL/min, which was the average measured flow rate during flame sampling. The simulations do not show any significant change (i.e., less than ±1%) in the concentrations of all the measured species (e.g., CO, C_2H_4, C_3H_6, etc.). However, the destruction of radicals (e.g., H, CH_3, OH, etc.) is observed in the simulations, and reactions forming low molecular weight oxygenate compounds (e.g., formaldehyde, acetaldehyde, ketene,

etc.) are present. A 5-20% (mol) increase in C_1-C_3 oxygenates is predicted, but most of these species are present in low PPM levels. These reactions in the sampling system are considered insignificant in the present study. However, these findings suggest that further analysis is required when using this sampling apparatus to study flames where oxygenated products are important.

Modeling uncertainties

Discrepancies between the model and experiments may also be attributed to uncertainties in the kinetic rate constants, thermochemical data, and transport parameters used in the model. Previous research [33-43] in opposed-flow laminar flames indicates that fuel reactivity is more sensitive to diffusivity estimates than to kinetic rate parameters because transport processes are rate controlling in these systems. Therefore, tuning rate and thermochemical constants to fit non-premixed flame data is not recommended. The testing and optimizations of kinetic parameters better suited for homogeneous combustion environments such as jet stirred reactors, premixed flames, and shock tube reactors. However, the adjustment of transport parameters to match the reactivity of the system is warranted.

Both Holley et al. [33] and Smallbone et al. [42] argue that the molecular diffusion model used in flame simulations is inaccurate because it assumes that the spherical potential of molecules is valid at elevated temperatures. They propose that the LJ transport parameters obtained at low temperature are not expected to accurately predict high temperature diffusivity. Smallbone et al. [42] concluded that a 50% increase in the binary diffusivity of *n*-heptane in N_2 was required to match their counter-flow flame ignition data. The diffusivity was increased by reducing in the collision diameter of *n*-heptane because diffusion is inversely related to the square of collision diameter. This uncertainty in fuel diffusivity may also play role in the present study, since the collision diameter for *n*-octane and 2-methylheptane were obtained from empirical correlations.

To test this hypothesis, the collision diameter of 2-methylheptane was arbitrarily reduced by 30% from 6.24 to 4.37 to account for a 50% increase in diffusivity. The results, shown in Figure 7, indicate improvements in the agreement between the model predictions and experiments. The predicted fuel profile is shifted towards the fuel port and more closely matches the experimental profile, which suggests that its transport is better modeled. The peak temperature, CO, CO_2, and minor species profiles are also better predicted by the model. Most notably, the ethylene predictions are improved; however, an over prediction of predicted acetylene concentration is observed. These results display the sensitivity of predicted species

and temperature profiles to the fuel diffusivity. Further investigation is required to create models that more accurately represent the transport of large fuel molecules in high temperature diffusion controlled environments.

Conclusions

The goal of this study was to improve our understanding of 2-methylheptane combustion. This was achieved by using experimental data for 2-methylheptane and *n*-octane in an opposed-flow diffusion flame to validate a novel high temperature chemical kinetic model. The experimental data indicate that the most abundant measured species were CO, CO_2, C_2H_4, and C_3H_6. Greater quantities of the 1-alkenes and ethylene were detected in the *n*-octane flame, while higher levels of 2-methylalkenes and propene were observed in the 2-methylheptane flame. The proposed chemical kinetic model exhibited excellent agreement with the experimental data. The reaction path analyses performed clearly indicate that H-atom abstraction reactions are the dominant route of fuel consumption. β-scission of the fuel radicals leads to formation of the species observed experimentally. The model shows that the higher levels of 2-methylalkenes in the 2-methylheptane flame can be attributed to the presence of the methylated portion of the molecule.

The proposed model is the first step towards developing a comprehensive chemical kinetic model for C_7 to C_{20} 2-methylalkanes with detailed low temperature and high temperature chemistry. This study verifies that the pathways and rate rules used for the high temperature reactions are acceptable for modeling the combustion of 2-methylalkanes. It is recommended that alkene chemistry be improved in the model to improve the prediction of diene species.

The uncertainty analysis presented in this study indicates that reactions in the sampling lines are negligible for the stable species measured in this study. However, further analysis is needed to identify the importance of these reactions on the concentrations of small oxygenate species. The predicted species and temperature profiles were found to be sensitive to fuel diffusivity, and an arbitrary 30% reduction in the collision diameter was found to improve the agreement between the model predictions and experiments. This study highlights the importance of further experimental and numerical studies to improve our understanding of transport processes in high temperature diffusion controlled environments.

Supplemental Material

This publication includes the following supplemental material:

1. Raw experimental data, modeling predictions, and corresponding graphs for 2-methylheptane in the opposed-flow diffusion flame. (.XLS format)
2. Raw experimental data, modeling predictions, and corresponding graphs for *n*-octane in the opposed-flow diffusion flame. (.XLS format)
3. The proposed chemical kinetic mechanism in CHEMKIN format. (.INP format)
4. The proposed thermodynamic datafile in CHEMKIN format. (.DAT format)
5. The proposed transport datafile in CHEMKIN format. (.DAT format)

Acknowledgements

The portion of this work supported by LLNL was performed under the auspoces of the U.S. Department of Energy by Lawrence Livermore National Laboratory under Contract DE-AC52-07NA27344. Add NAVY acknowledgement. The work at University of Toronto was supported by the Natural Science and Engineering Research Council of Canada (NSERC).

References

1. D. Leckel, Energy Fuels. 23 (2009) 2342–2358.
2. T. Edwards, D. Minus, W. Harrison, E. Corporan, M. DeWitt, S. Zabarnick, L. Balster, AIAA-2004-3885.
3. B.L. Smith, T.J. Bruno, J. Propulsion 24 (3) (2008) 619-623.
4. B.L. Smith, T.J. Bruno, Ind. Eng. Chem. Res. 46 (1) (2007) 310-320.
5. M.L. Huber, B.L. Smith, L.S. Ott, T.J. Bruno, Energy Fuels 22 (2008), 1104-1114.
6. P. Gokulakrishnan, M.A. Klassen, R.J. Roby, ASME Turbo Expo (2008) #GT2008-51211, Berlin, Germany
7. M. Colket, T. Edwards, S. Williams, N. Cernansky, D.L Miller, et al., 45th AIAA Aerospaces Sciences Meeting and Exhibit (2007) #AIAA 2007-770, Reno, Nevada.
8. R. Wilk, W.J. Pitz, C.K. Westbrook, S. Addagarla, D.L. Miller, N.P. Cernansky, R.M. Green, Proc. Combust. Inst. 23 (1990) 1047-1053.
9. T. Ogura, Y. Nagumo, A. Miyoshi, M. Koshi, Energy Fuels, 21 (2007) 130-135.
10. M.A. Oehlschlaeger, D.F. Davidson, J.T. Herbon, R.K. Hanson, Int. J. Chem. Kinet. 36 (2) (2004) 67-78.

11. D. Healy, N.S. Donato, C.J. Aul, E.L. Petersen, C.M. Zinner, G. Bourque, H.J. Curran, Combust Flame 157 (2010) 1540-1551.

12. A. Burcat, E. Olchanski, C. Sokolinski, Combust. Sci. and Tech. 147 (1999) 1-37.

13. C.K. Westbrook, W.J. Pitz, H.J. Curran, J. Boercker, E. Kunrath, Int. J. Chem. Kinet. 33 (12) (2001) 868-877.

14. C.K. Westbrook, W.J. Pitz, J.E. Boercker, H.J. Curran, J.F. Griffiths, C. Mohamed, M. Ribacour, Proc. Combust. Inst. 29 (2002) 1311-1318.

15. J.F. Griffiths, J.P. MacNamara, C.G.W. Sheppard, D.A. Turton, B.J. Whitaker, Fuel 81 (2002) 2219–2225.

16. E.J. Silke, H.J. Curran, J.M. Simmie, Proc. Combust. Inst. 30 (2005) 2639-2647.

17. M.S.P. Kahandawala, M.J. DeWitt, E. Corporan, S.S. Sidhu, Energy Fuels 22 (2008) 3673-3679.

18. S. M. Sarathy, M. J. Thomson, C. Togbe, P. Dagaut, F. Halter, C. Mounaim-Rousselle, Combust. Flame 156 (2009) 852-864.

19. C.S. Mcenally, U.O. Koylu, L.D. Pfefferle, D.E. Rosner, Combust. Flame 109 (1997) 701-720.

20. C.R. Shaddix, Proc. 33rd National Heat Transfer Conf. (1999) Albuquerque, New Mexico.

21. D. Bradley, A.G. Entwistle, Brit. J. Appl. Phys. 12 (1961) 708-711.

22. D. R. Lide, ed., CRC Handbook of Chemistry and Physics, Internet Version 2007, (87th Edition), <http:/www.hbcpnetbase.com>, Taylor and Francis, Boca, Raton, FL, 2007.

23. R. J. Kee, F. M. Rupley, J. A. Miller, M. E. Coltrin, J. F. Grcar, E. Meeks, H. K. Moffat, A. E. Lutz, G. Dixon-Lewis, M. D. Smooke, J. Warnatz, G. H. Evans, R. S. Larson, R. E. Mitchell, L. R. Petzold, W. C. Reynolds, M. Caracotsios, W. E. Stewart, P. Glarborg, C. Wang, C. L. McLellan, O. Adigun, W. G. Houf, C. P. Chou, S. F. Miller, P. Ho, P. D. Young, D. J. Young, D. W. Hodgson, M. V. Petrova and K. V. Puduppakkam, "CHEMKIN-PRO Release 15082," Reaction Design, Inc, San Diego, CA, 2008.

24. C.K. Westbrook, W.J. Pitz, O. Herbinet, H.J. Curran, E.J. Silke, Combust. Flame 156 (2009) 181-199.

25. M. Mehl, H. J. Curran, W. J. Pitz , C. K. Westbrook, European Combustion Meeting, Vienna, Austria, 2009.

26. M. Mehl, W. J. Pitz, M. Sjöberg, J. E. Dec, SAE 2009 International Powertrains, Fuels and Lubricants Meeting, SAE Paper No. 2009-01-1806, Florence, Italy.

27. H.J. Curran, P. Gaffuri, W.J. Pitz, C.K. Westbrook, Combust. Flame 114 (1998) 149-177.
28. H.J. Curran, P. Gaffuri, W.J. Pitz, C.K. Westbrook, Combust. Flame 129 (2002) 253-280.
29. E.R. Ritter, J.W. Bozelli, Int. J. Chem. Kin. 23 (1991) 767-778.
30. S.W. Benson, Thermochemical Kinetics (2nd ed.), Wiley, New York (1976).
31. F.M. Mourits, F.H.A. Rummens, Can. J. Chem. 55 (1977) 3007-3020.
32. L.S. Tee, S. Gotoh, W.E. Stewart, Ind. Eng. Chem. Fundam. 5 (3) (1966) 356-363.
33. A.T. Holley, Y. Dong, M.G. Andac, F.N. Egolfopoulos, Combust. Flame 144 (2006) 448-460.
34. P.J. Linstrom, W.G. Mallard, Eds., NIST Chemistry WebBook, NIST Standard Reference Database Number 69, 2005, National Institute of Standards and Technology, Gaithersburg MD, 20899 (http://webbook.nist.gov).
35. A.L. McClellan, Tables of Experimental Dipole Moments, Freeman, San Francisco, 1963.
36. N. Hansen, T.A. Cool, P.R. Westmoreland, K. Kohse-Hoinghaus, Prog. Energy Combust. Sci. 35 (2009) 168-191.
37. S.M. Sarathy, M.J. Thomson, W.J. Pitz, T. Lu, Proc. Combust. Inst. (2010), doi:10.1016/j.proci.2010.06.058.
38. G. Dayma, S.M. Sarathy, C. Togbe, C. Yeung, M.J. Thomson, P. Dagaut, Proc. Combust. Inst. (2010), doi:10.1016/j.proci.2010.05.024.
39. M. Mehl, G. Vanhove, W.J. Pitz, E. Ranzi, Combustion and Flame 155 (2008) 756–772.
40. M. Mehl, W.J. Pitz, C.K. Westbrook, K. Yasunaga, C. Conroy, H.J. Curran, Proc. Combust. Inst. (2010), doi:10.1016/j.proci.2010.05.040.
41. M.G. Andac, F.N. Egolfopoulos, Proc. Combust. Inst. (2007) 1165-1172.
42. A.J. Smallbone, W. Liu, C.K. Law, X.Q. You, H. Wang, Proc. Combust. Inst. (2009) 1245-1252.
43. A.T. Holley, X.Q. You, E. Dames, H. Wang, F.N. Egolfopoulos, Proc. Combust. Inst. 32 (2009) 1157-1163.

List of Figures

Figure 1 - Structure of 2-methylheptane

Figure 2 – Experimental and computed profiles obtained from the oxidation of 2-methylheptane in an atmospheric opposed-flow flame (1.86% fuel, 42% O_2).

Figure 3 - Experimental and computed profiles obtained from the oxidation of 2-methylheptane in an atmospheric opposed-flow flame (1.86% fuel, 42% O2).

Figure 4 - Reaction pathway diagram for 2-methylheptane oxidation in the opposed-flow diffusion flame at T=805K (italicized text) and T=1185K (bold text)

Figure 5 - Reaction pathway diagram for n-octane oxidation in the opposed-flow diffusion flame at T=805K (italicized text) and T=1185K (bold text)

Figure 6 – Diagram used for simulating the species sampling system
Figure 7- Experimental and computed profiles obtained from the oxidation of 2-methylheptane in an atmospheric opposed-flow flame (1.86% fuel, 42% O2) using a 30% reduction in 2-methylheptane collision diameter.

List of Tables

Table 1 - Peak measured and predicted temperatures and concentrations in the opposed-flow diffusion flame. Italicized numbers are measured values, bold numbers represent predicted values, and underlined numbers are the ratio of measured to predicted.

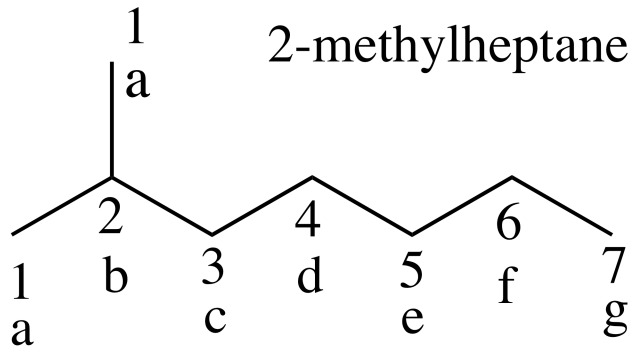

Figure 1 – Structure of 2-methylheptane

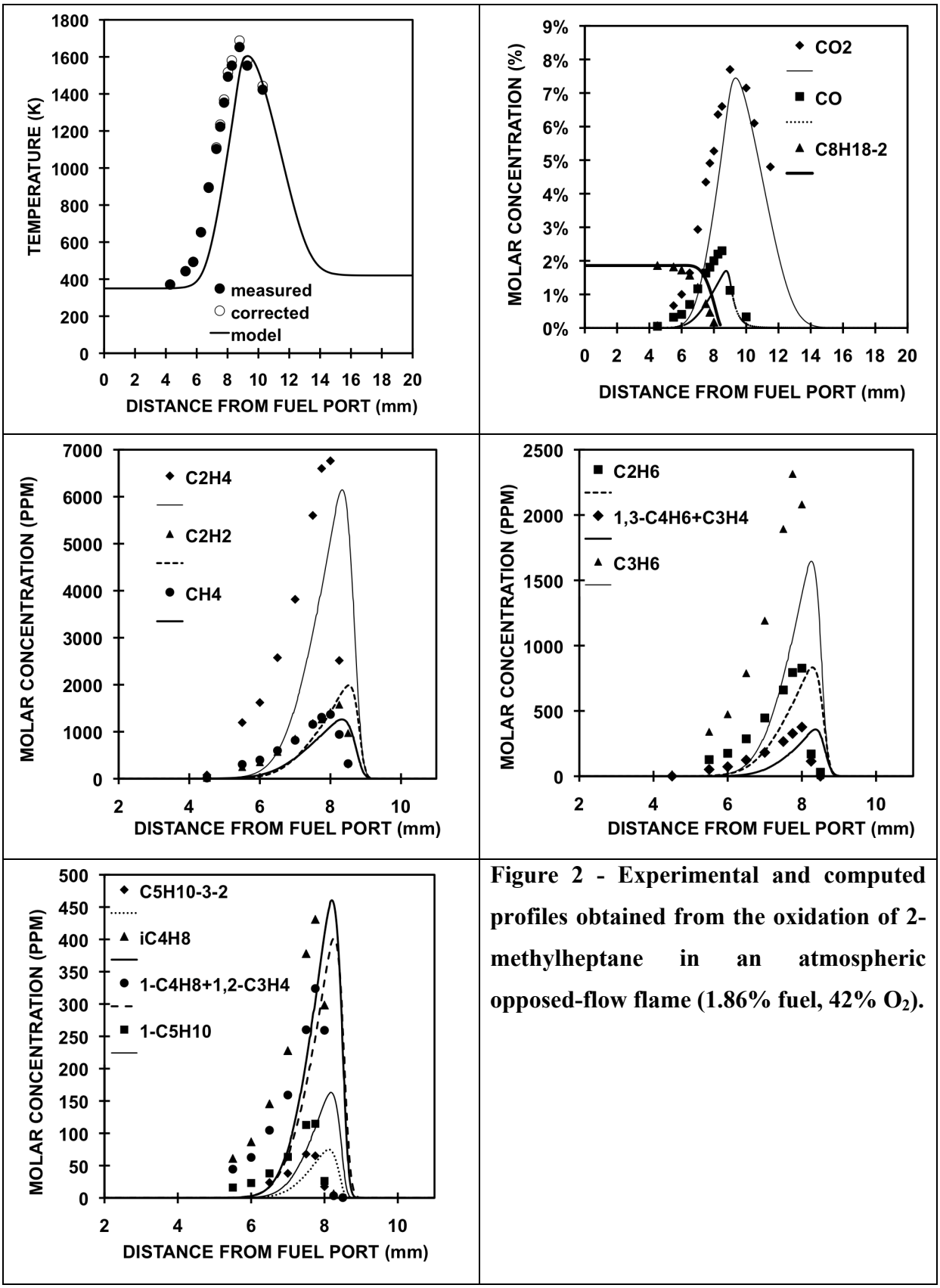

Figure 2 - Experimental and computed profiles obtained from the oxidation of 2-methylheptane in an atmospheric opposed-flow flame (1.86% fuel, 42% O_2).

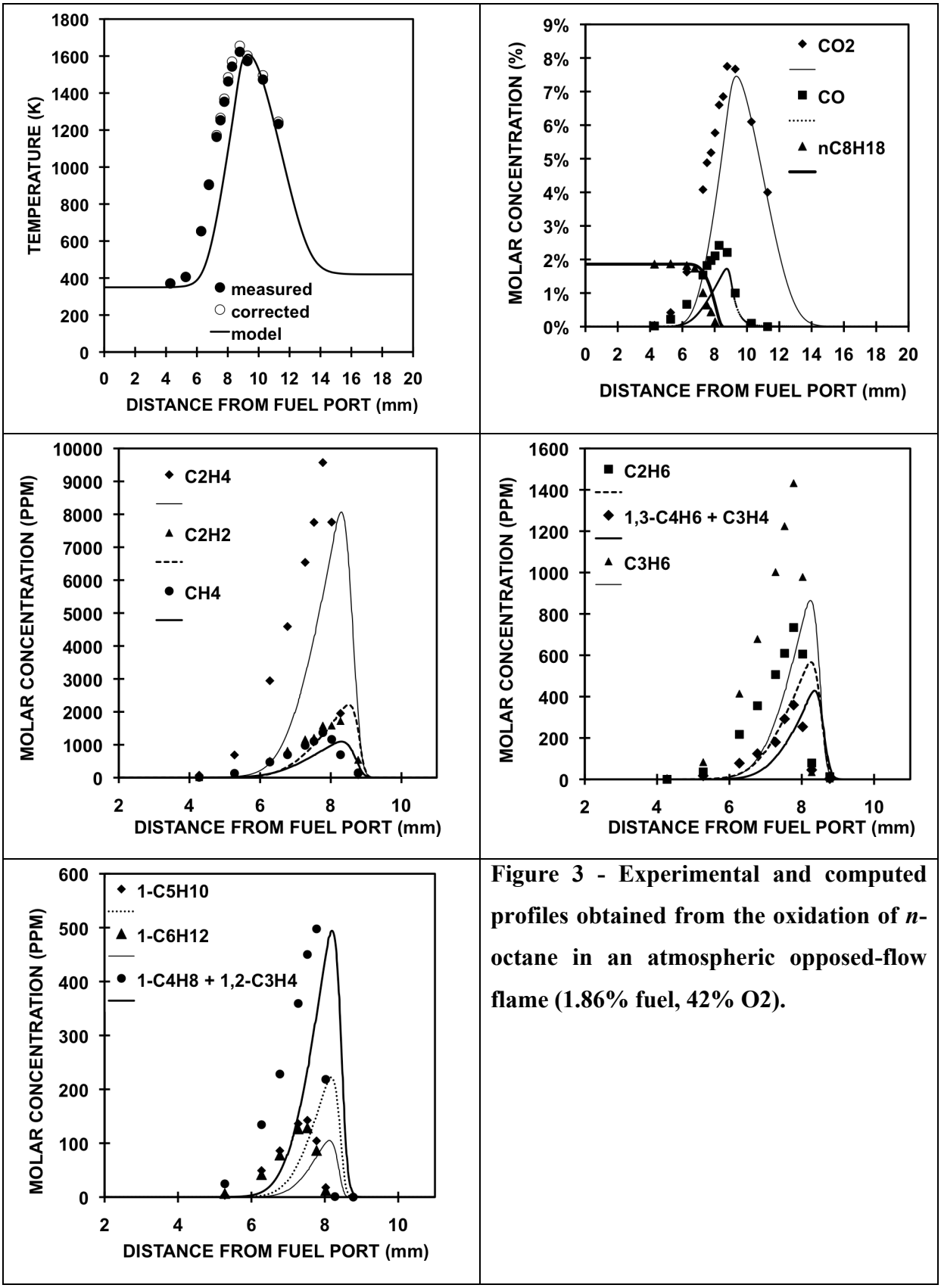

Figure 3 - Experimental and computed profiles obtained from the oxidation of *n*-octane in an atmospheric opposed-flow flame (1.86% fuel, 42% O2).

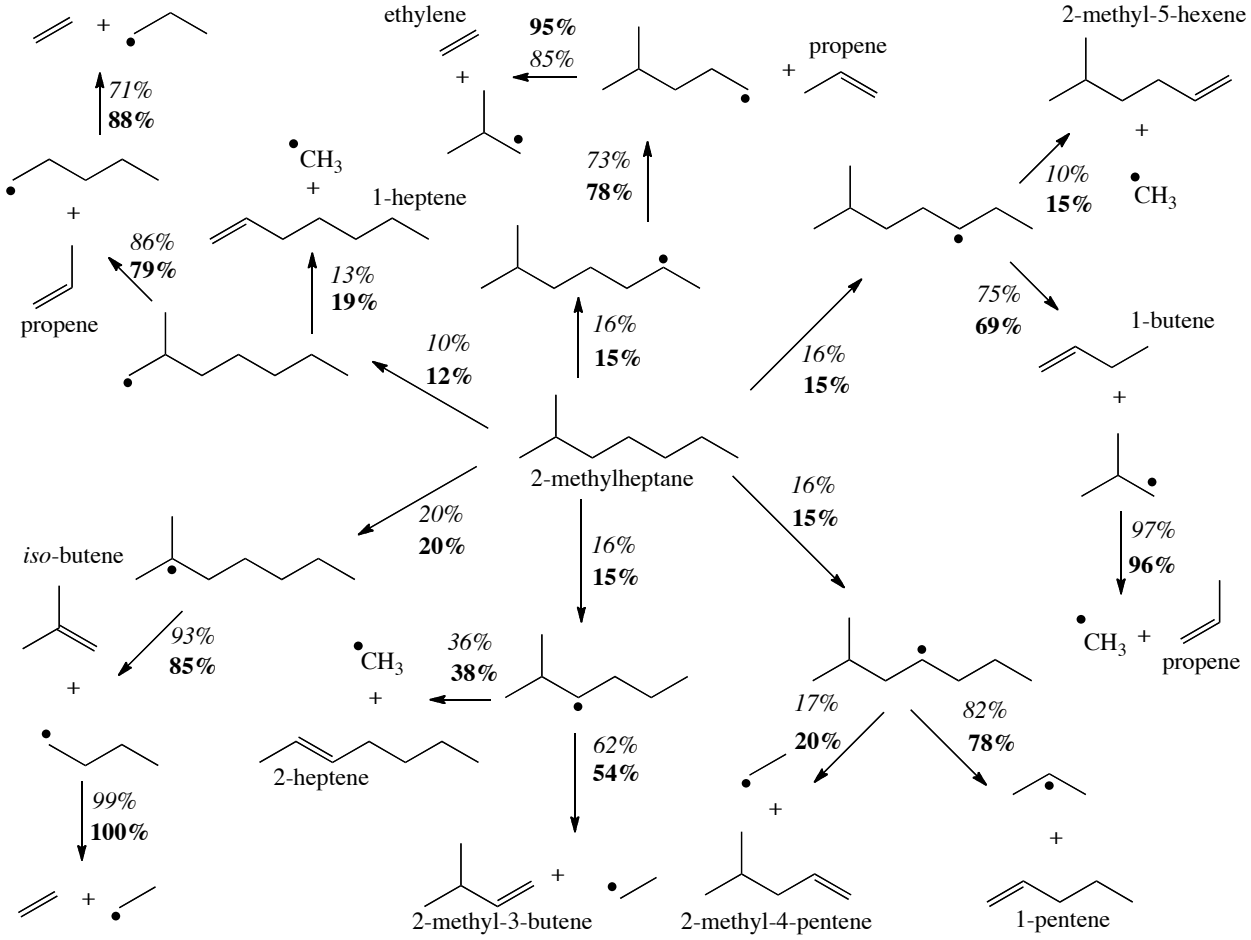

Figure 4 - Reaction pathway diagram for 2-methylheptane oxidation in the opposed-flow diffusion flame at T=805K (italicized text) and T=1185K (bold text)

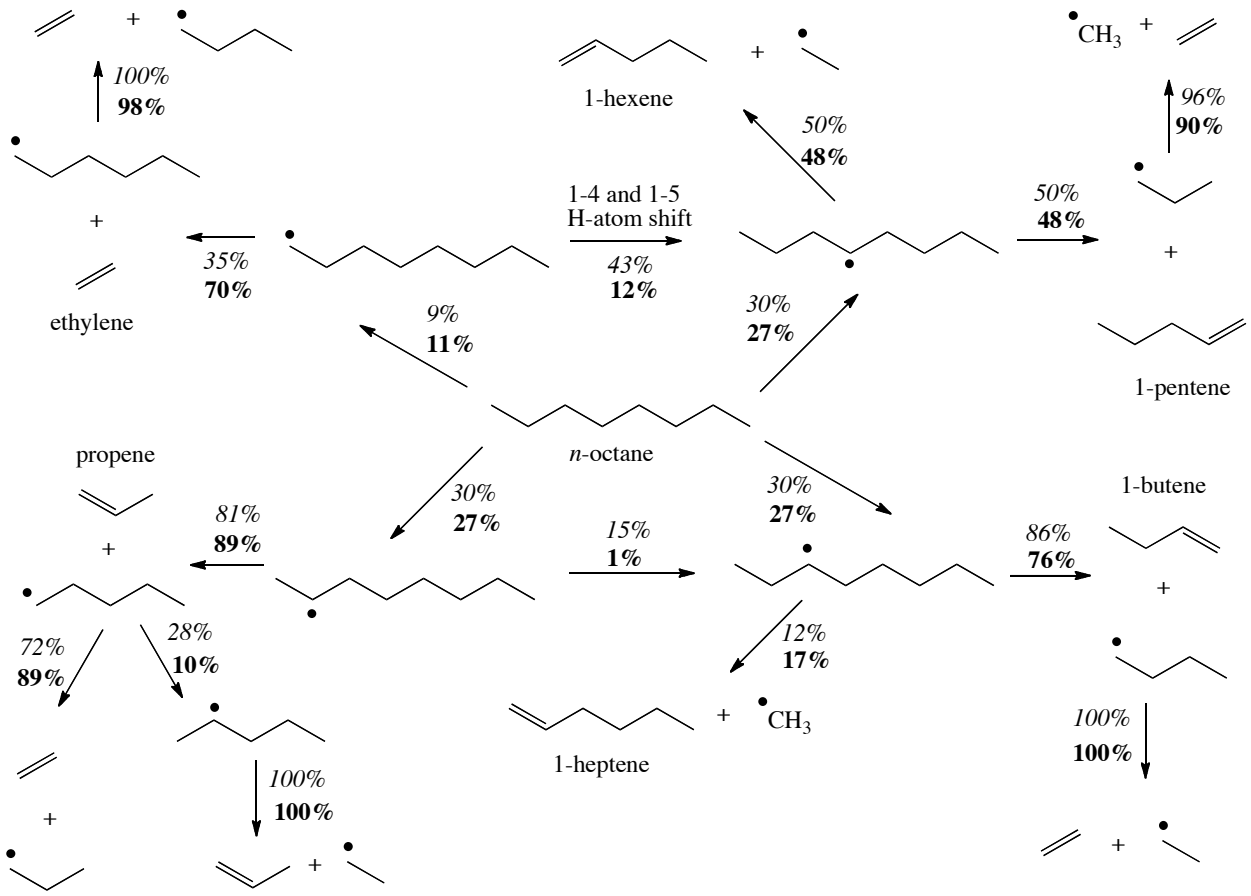

Figure 5 - Reaction pathway diagram for *n*-octane oxidation in the opposed-flow diffusion flame at T=805K (italicized text) and T=1185K (bold text)

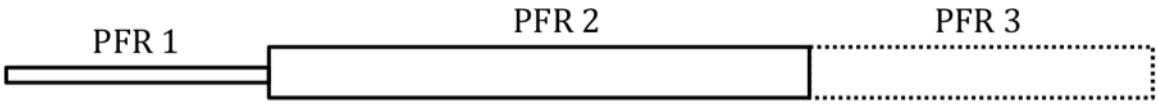

microprobe	suction line	compression line
0.20 mm ID	6.35 mm ID	6.35 mm ID
5 cm length	2 m length	1 m length
P = 5 kPa	P = 5 kPa	P = 101.3 kPa
T = 400 K	T = 400 K	T = 400 K

not to scale

Figure 6 – Diagram used for simulating the species sampling system

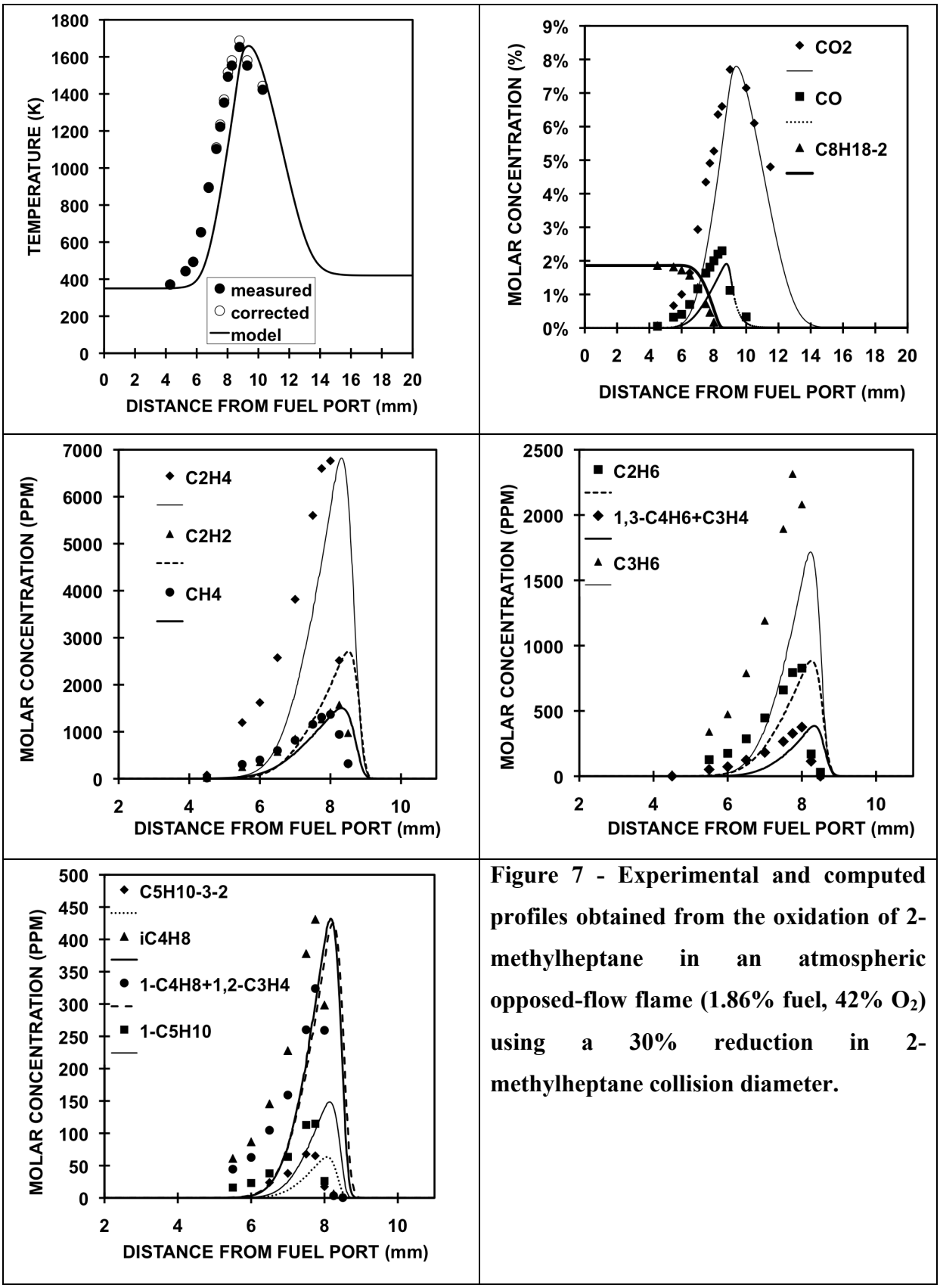

Figure 7 - Experimental and computed profiles obtained from the oxidation of 2-methylheptane in an atmospheric opposed-flow flame (1.86% fuel, 42% O_2) using a 30% reduction in 2-methylheptane collision diameter.

Table 1 - Peak measured and predicted temperatures and concentrations in the opposed-flow diffusion flame. Italicized numbers are measured values, bold numbers represent predicted values, and underlined numbers are the ratio of measured to predicted.

Measured Parameter	nC_8H_{18} / n-octane	C_8H_{18}-2 / 2-methylheptane
Temperature (K)	*1655*	*1688*
	1606	**1604**
	1.0	1.0
CO_2 / carbon dioxide (%)	*7.75*	*7.70*
	7.46	**7.45**
	1.0	1.0
CO / carbon monoxide (%)	*2.42*	*2.30*
	1.72	**1.70**
	1.4	1.4
CH_4 / methane (PPM)	*1369*	*1368*
	1096	**1261**
	1.2	1.1
C_2H_6 / ethane (PPM)	*734*	*827*
	566	**833**
	1.3	1.0
C_2H_4 / ethylene (PPM)	*9571*	*6763*
	8068	**6146**
	1.2	1.1
C_2H_2 / acetylene (PPM)	*1582*	*1575*
	2215	**1987**
	0.7	0.8
C_3H_6 / propene (PPM)	*1432*	*2314*
	865	**1646**
	1.7	1.4
1-C_4H_8 + 1,2-C_3H_4 /	*498*	*431*
1-butene + 1,2-propadiene (PPM)	**494**	**400**
	1.0	1.1
1,3-C_4H_6 + C_3H_4 /	*359*	*376*
1,3-butadiene + propyne (PPM)	**428**	**358**
	0.8	1.1
iC_4H_8 / *iso*-butene (PPM)	*< LOD*	*324*
	2	**460**
	N/A	0.7
1-C_5H_{10} / 1-pentene (PPM)	*142*	*114*
	222	**163**
	0.6	0.4
C_5H_{10}-3-2 / 2-methyl-3-butene (PPM)	*< LOD*	*68*
aka 3-methyl-1-butene	**0**	**75**
	N/A	0.9
1-C_6H_{12} / 1-hexene (PPM)	*129*	*< LOD*
	105	**1**
	1.2	N/A
C_6H_{12}-4-2/ 2-methyl-4-pentene (PPM)	< LOD	*40*
aka 4-methyl-1-pentene	0	**30**
	N/A	1.3